Journal Pre-proofs

Ultra-small platinum nanoparticles segregated by nickle sites for efficient ORR and HER processes

Lvhan Liang, Huihui jin, Huang Zhou, Bingshuai Liu, Chenxi Hu, Ding Chen, Jiawei Zhu, Zhe Wang, Hai-Wen Li, Suli Liu, Daping He, Shichun Mu

PII: S2095-4956(21)00320-X
DOI: https://doi.org/10.1016/j.jechem.2021.05.033
Reference: JECHEM 1986

To appear in: *Journal of Energy Chemistry*

Received Date: 19 April 2021
Revised Date: 17 May 2021
Accepted Date: 22 May 2021

Please cite this article as: L. Liang, H. jin, H. Zhou, B. Liu, C. Hu, D. Chen, J. Zhu, Z. Wang, H-W. Li, S. Liu, D. He, S. Mu, Ultra-small platinum nanoparticles segregated by nickle sites for efficient ORR and HER processes, *Journal of Energy Chemistry* (2021), doi: https://doi.org/10.1016/j.jechem.2021.05.033

Ultra-small platinum nanoparticles segregated by nickle sites for efficient ORR and HER processes

Lvhan Liang[a,b,1], Huihui jin[a,c,1], Huang Zhou[a], Bingshuai Liu[a], Chenxi Hu[a], Ding Chen[a], Jiawei Zhu[a], Zhe Wang[c], Hai-Wen Li[d], Suli Liu[e*], Daping He[a,c*], Shichun Mu[a,b*]

[a] *State Key Laboratory of Advanced Technology for Materials Synthesis and Processing, Wuhan University of Technology, Wuhan 430070, Hubei, China*
[b] *Foshan Xianhu Laboratory of the Advanced Energy Science and Technology Guangdong Laboratory, Xianhu Hydrogen Valley, Foshan 528200, Guangdong, China*
[c] *Hubei Engineering Research Center of RF-Microwave Technology and Application, Wuhan University of Technology, Wuhan 430070, Hubei, China*
[d] *Platform of Inter/Transdisciplinary Energy Research, International Research Center for Hydrogen Energy, International Institute for Carbon-Neutral Energy Research, Kyushu University, Fukuoka, 819-0395, Japan*
[e] *Key Laboratory of Advanced Functional Materials of Nanjing, Nanjing Xiaozhuang University, Nanjing 211171, Jiangsu, China*
[1] These authors contributed equally to this work.
[*]Corresponding authors.

E-mail addresses: msc@whut.edu.cn (S. Mu); hedaping@whut.edu.cn (D. He); niuniu_410@126.com (S. Liu)

ABSTRACT

In the electrochemical process, Pt nanoparticles (NPs) in Pt-based catalysts usually agglomerate due to Oswald ripening or lack of restraint, ultimately resulting in reduction of the active sites and catalytic efficiency. How to uniformly disperse and firmly fix Pt NPs on carbon matrix with suitable particle size for catalysis is still a big challenge. Herein, to prevent the agglomeration and shedding of Pt NPs, Ni species is introduced and are evenly dispersed in the surface of carbon matrix in the form of Ni-N-C active sites (Ni ZIF-NC). The Ni sites can be used to anchor Pt NPs, and then effectively limit the further growth and agglomeration of Pt NPs during the reaction process. Compared with commercial Pt/C catalyst, Pt@Ni ZIF-NC, with ultralow Pt loading (7 wt.%) and ideal particle size (2.3 nm), not only increase the active center, but also promotes the catalysis kinetics, greatly improving the ORR and HER catalytic activity. Under acidic conditions, its half-wave potential (0.902 V) is superior to commercial Pt/C (0.861 V), and the mass activity (0.38 A per mg Pt) at 0.9 V is 4.7 times that of Pt/C (0.08 A per mg Pt). Besides, it also shows outstanding HER performance. At 20 and 30mV, its mass activity is even 2 and 6 times that of Pt/C. Whether it is under ORR or HER conditions, it also shows excellent durability. These undoubtedly indicate the realization of dual-functional catalysts with low-Pt and high-efficiency properties.

Keywords: Oxygen reduction reaction; Hydrogen evolution reaction; Zeolitic Imidazolate Frameworks; Nickle site; Pt nanoparticles

1. Introduction

Nowadays, to achieve sustainable and green development, it is necessary to replacing the conventional fossil energy via the use of renewable energy. As an efficient energy conversion solution device, proton exchange membrane fuel cells (PEMFCs) has aroused new interest of researchers [1]. During the operation of PEMFCs, the reaction rate of the oxygen reduction reaction (ORR) at the cathode is very slow, which has to employ the expensive Pt catalyst to drive the ORR process. At the same time, to produce pure hydrogen as the main fuel of PEMFCs, Pt is also an efficient catalyst for the anode hydrogen evolution reaction (HER) in the process of electrolyzing water. However, the slow cathodic oxygen reduction kinetics and insufficient pure hydrogen product as anode fuel are the main factors limiting the development of PEMFCs [2–4]. Hence, developing effective catalysts for ORR and HER is imperative [5–9]

Until now, Pt-based catalysts have been the most effective catalysts for ORR and HER. However, commercial Pt catalysts such as Pt/C for ORR and HER also has some shortcomings [10–14], such as high Pt loading, poor stability and easy agglomeration, which severely limits its large-scale use. In addition, in the future development of PEMFCs, reducing the dosage of Pt and improving the stability of catalysts are of great important [15–17]. Thus, recently some highly efficient low-Pt catalysts have been developed by means of changing the form of Pt (Pt nanowires, Pt nanoframes, Pt nanocages, etc.), alloying with non-noble metals, and replacing different carriers [18–23].

Regardless of the aforementioned methods, the most important thing is to effectively control the amount of Pt and achieve high-efficiency catalysis. However, the preparation conditions for changing the fine structure of Pt and alloying Pt are severe, and the size of Pt particles is difficult to control. The method of selecting

suitable support is much more convenient in comparison [24–26]. Metal organic frameworks (MOFs) as a material developed recently, have been widely developed and applied in the fields of catalysts. Zeolite imidazole frameworks (ZIFs), as a kind of MOFs, are very suitable as a precursor of catalytic material because of high designability, small volume, large specific surface area, rich carbon and nitrogen content, and pore of different sizes [27–32]. When doped with transition metals (Fe, Co, Zn, Ni, etc.) and annealed at high temperatures, it will produce a large number of active sites and excellent conductivity, which is promising in catalysis applications [33]. In addition, these characteristics make ZIFs-derived materials also suitable as supports for noble metals [34,35]. For example, Chen et al. synthesized a porous N-doped carbon-based catalyst with rich Fe single-atom sites derived from ZIF, which showed a high- oxygen reduction performance under alkaline conditions [3]. Yuan et al. chose Zn-Co ZIF to produce Co sites by pyrolysis, then impregnated the Ru source, the obtained material was further thermally reduced to get Ru@Co-SAs/N-C. Compared with commercial Pt/C, it has better activity and stability in HER [36].

In this work, we prepare a ZIF-derived high-efficiency bifunctional low-Pt catalyst (Pt@Ni ZIF-NC). It possesses ultra-small and uniformly dispersed Pt NPs by dispersing Ni sites on the porous N-doped carbon materials (ZIF-NC) to restrict the growth of Pt. Due to the existence and interaction of Pt and Ni dual active sites, Pt@Ni ZIF-NC shows high ORR and HER activity under acidic conditions. Since Pt NPs are fixed and uniformly dispersed by Ni sites, the catalyst also exhibits excellent stability.

2. Experimental

2.1. Synthesis of Ni NPs

257 mg $Ni(acac)_2$ with 15 mL oleylamine and 0.32 mL oleic acid were mixed under a

nitrogen atmosphere, mix, and then heat to 120 °C within 15 minutes to obtain the green solution. Then stir the solution at 120 °C for 90 min. After that, the solution was cooled to 90 °C, added 2 mL oleylamine in which 264 mg of BTB was dissolved. It can be observed that the solution has changed from green to brown. Then the solution was kept at 110 °C for 60 min and then cool down naturally. 30 mL of ethanol was added and the product was separated by centrifugation. The product was then dispersed in 10 mL of n-hexane for futher use.

2.2. Synthesis of ZIF-8

2-methylimidazole (3.08g) and $Zn(NO_3)_2 \cdot 6H_2O$ (2.79g) was dissolved in 75 mL methanol respectively, and stir them for five minutes. Then, Add the former to the latter while stirring evenly, the mixture was stirred at 35 °C for 4 h. The resultant product was centrifuged and washed by methanol, and then dried in vacuum at 70 °C for 10 h to obtain ZIF-8 powder.

2.3. Synthesis of ZIF-NC and Ni ZIF-NC

The as-prepared ZIF-8 was pyrolyzed at 900 °C for 3 h in the tube furnace with a rate of 5 °C min^{-1} (all subsequent heating rates are the same) to finally get ZIF-NC.

50 mg ZIF-NC was dispersed in 25 mL hexane, sonicate for 5 minutes, then 60 μL Ni NPs solution was added to it and sonicate for 5 minutes, the mixture was under strong agitation for 12 hours at 25 °C. Finally, the product was centrifuged and dry under vacuum at 70 °C. The resulting product undergoes the above-mentioned ZIF-NC steps to obtain Ni ZIF-NC.

2.4. Synthesis of H_2PtCl_6@ZIF-NC and H_2PtCl_6@Ni ZIF-NC

ZIF-NC (50 mg) and Ni ZIF-NC (50 mg) were respectively dispersed in 5 mL H_2PtCl_6 solution (60 mg mL^{-1}). After stirring at 70 °C for 10 h, the products were centrifuged and rinsed by ethanol, and finally dried in vacuum at 70 °C for 10 h.

2.5. Synthesis of Pt@ZIF-NC and Pt@Ni ZIF-NC

The as prepared H_2PtCl_6@ZIF-NC and H_2PtCl_6@Ni ZIF-NC were pyrolyzing under an 5% H_2/Ar atmosphere at 250 °C for 1 h to finally obtain Pt@ZIF-NC and Pt@Ni ZIF-NC.

3. Results and discussion

3.1. Structural characterization

The synthesis process of Pt@Ni ZIF-NC is represented in Fig. 1. Ni NPs and ZIF-8 were first synthesized. Subsequently Ni NPs were dissolved in n-hexane for further use, ZIF-8 was heated to 900 °C under nitrogen atmosphere, and naturally cooled to obtain N-doped carbon matrix (ZIF-NC). Then the prepared Ni NPs was added to the ZIF-NC, after uniform mix at room temperature to make it adhere to the ZIF-NC, and then annealing at high temperatures to disperse the Ni NPs into uniform and tiny Ni sites, Ni ZIF-NC was formed. After that, Ni ZIF-NC was reacted with H_2PtCl_6 solutions at 70 °C to get H_2PtCl_6@Ni ZIF-NC. Finally, H_2PtCl_6@Ni ZIF-NC was reduced at 250 °C for 1 h under 5% H_2/Ar atmosphere to obtain Pt NPs anchored by Nickle site (Pt@Ni ZIF-NC). The same experiment was performed on ZIF-8 without Ni NPs, and Pt loaded N-doped carbon matrix (Pt@ZIF-NC) were obtained, respectively.

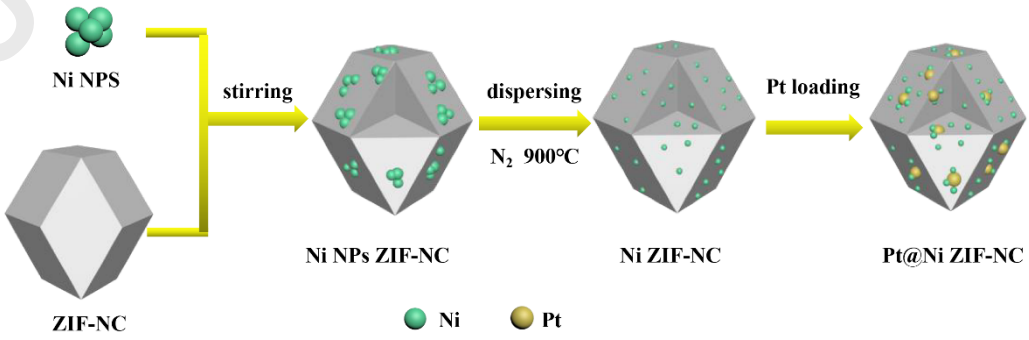

Fig. 1. Schematic diagram of the synthesis for Pt@Ni ZIF-NC.

The scanning electron microscope (SEM) (Fig. 2a, d) shows that both Pt@ZIF-NC and Pt@Ni ZIF-NC own a regular rhombic dodecahedron morphology and are uniform in size. And from the transmission electron microscope (TEM) images (Figs. 2b, e and S1 and S2), Pt NPs in Pt@Ni ZIF-NC have a uniform size distribution with smaller particles, while Pt NPs in Pt@ZIF-NC are scattered and partly agglomerated. Through further observation of the enlarged TEM and statistics of the particle size for Pt NPs, it can be found that the distribution of the Pt NPs in Pt@ZIF-NC is relatively wide, the average particle size is 3.7 nm (Fig. 2c). While the Pt NPs in Pt@Ni ZIF-NC are mainly concentrated at about 2 nm, with the average particle size of 2.3 nm (Fig. 2f). To further evidence the metal nanoparticle is the Pt in Pt@Ni ZIF-NC, the high-resolution TEM (HRTEM) was used for observation. As shown in Fig. 2(g, h), Pt NPs in Pt@Ni ZIF-NC are fixed in the carbon matrix, and the distance between the two crystal planes of Pt was measured to be 0.23 nm, which corresponds to the (111) plane of Pt. EDX element mappings (Fig. 2i–m) further prove the uniform distribution of each element in Pt@Ni ZIF-NC, especially for Pt, indicating that there is hardly no agglomeration of Pt NPs in Pt@Ni ZIF-NC. The ICP test shows 7 wt.% Pt loading in Pt@Ni ZIF-NC, indicating far below the 20% of commercial Pt/C (Table S1).

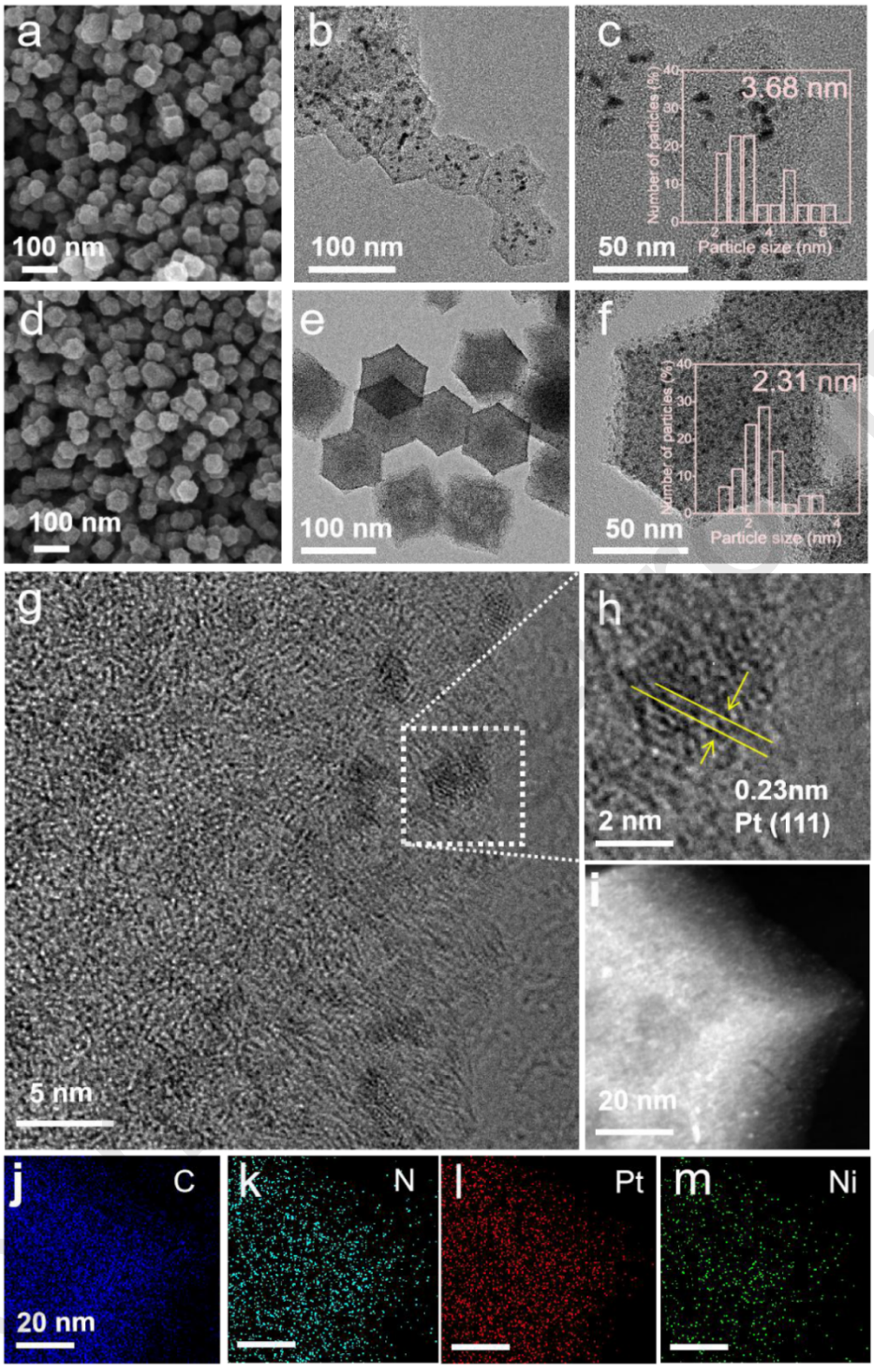

Fig. 2. (a) SEM and (b) TEM and (c) Magnified TEM (inset: Pt NPs particle size statistics chart) images of Pt@ZIF-NC, (d) SEM and (e) TEM and (f) Magnified TEM images of Pt@Ni ZIF-NC (inset: Pt NPs particle size statistics chart). (g) HRTEM and (h) Magnified HRTEM of Pt@Ni ZIF-NC. (i–m) HAADF-STEM with EDX elemental

mapping of Pt@Ni ZIF-NC.

X-ray diffraction (XRD) pattern (Fig. 3a) reveals that Pt@Ni ZIF-NC and Ni ZIF-NC possess a broad peak at approximately 24.8°, which is attributed to the C (002) plane. The diffraction peaks located at 2θ = 39.8°, 46.5°, and 67.7° belong to (111), (200), and (220) planes of Pt, respectively, indicating the crystal structure of Pt NPs in Pt@Ni ZIF-NC is face-centered cubic (fcc). There is no obvious Ni peak, indicating that most of the Ni NPs are dispersed into tiny Ni sites. According to Raman spectra (Fig. 3b), the I_D/I_G of Pt@Ni ZIF-NC is 1.02, while that of Pt@ZIF-NC is 0.96, indicating that more defects were produced in the carbon matrix surface during the process of forming Ni sites from dispersed Ni NPs.

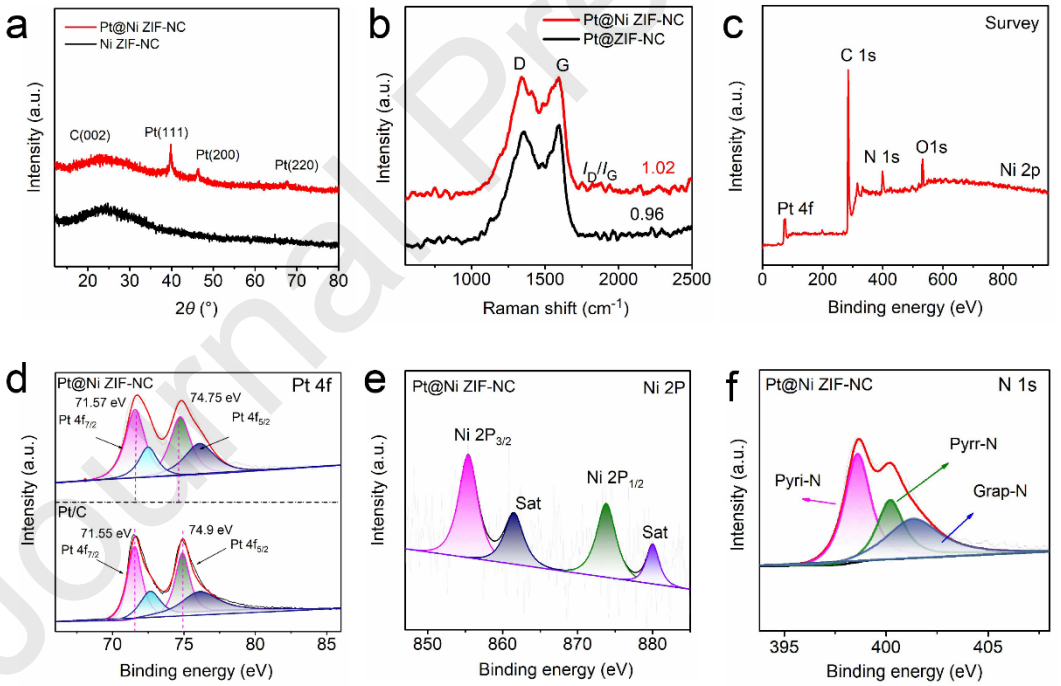

Fig. 3. (a) XRD pattern of Pt@Ni ZIF-NC and Ni ZIF-NC. (b) Raman spectra of Pt@Ni ZIF-NC and Pt@ZIF-NC. (c) XPS survey scan of Pt@Ni ZIF-NC. (d) Pt 4f spectrum of Pt@Ni ZIF-NC and Pt/C. (e) Ni 2p spectrum of Pt@Ni ZIF-NC. (f) N 1s spectrum of Pt@Ni ZIF-NC.

The X-ray photoelectron spectroscopy (XPS) of Pt@Ni ZIF-NC proves the existence of Pt, Ni, C, N and O (Fig. 3c). Besides, the small Ni peak is caused by the lower total content of Ni elements, and it exists basically in the form of tiny Ni sites. Fig. 3(d) shows the Pt 4f spectra of Pt@Ni ZIF-NC and Pt/C. The binding energy of Pt@Ni ZIF-NC at the Pt $4f_{5/2}$ peak has a lower negative shift (0.15 eV) when compared with Pt/C, indicating that the electronic structure of Pt on the surface of Pt@Ni ZIF-NC was indeed modified by the diffused Ni sites. Compared to Pt@ZIF-NC, there is also a slight negative shift (Fig. S3), exhibiting that after loading Pt on Ni ZIF-NC, the obtained electronic structure can be changed, and the downward shift of the d-band center causes the reduction of the electron return of the Pt 5d orbital. So the ORR would be accelerated [38,39]. Compared with Pt/C, a negative shift (0.15 eV) of binding energy is adverted for the Pt 4f doublet on Pt@Ni ZIF-NC, because of the effect of Ni sites and porous N-doped carbon carrier on Pt NPs. In theory, Pt possesses higher electronegativity compared to Ni, hence the Pt in Pt@Ni ZIF-NC should be more metallic compared to individual Pt NPs, and the binding energy should exhibit a negative shift, which is accord with the XPS results, sustaining the structure of Pt@Ni ZIF-NC [37]. Fig. 3(e) shows that the $2p_{3/2}$ and Ni $2p_{1/2}$ peaks of Ni are located at 855.4 and 873.4 eV, respectively, and the two satellite peaks are located at 861.7 and 880.2 eV, respectively [38]. There are three dividing peaks of the N 1s XPS spectra in Pt@Ni ZIF-NC, representing pyridinic N (398.7 eV), pyrrolic N (400.2 eV), and graphitic N (401.3 eV), respectively [27,40,41]. This shows that N was successfully doped into the carbon matrix. Fig. 3(f) and Table S2

show the presence of a large amount of pyridine N and graphite N, conducive to increase the active site and limiting current density of the catalyst, respectively.

3.2. Electrocatalytic performance towards ORR

The Pt loadings on the electrode of Pt@Ni ZIF-NC, Pt@ZIF-NC and Pt/C are 3.5, 4.7 and 6 μg, respectively. Fig. 4(a) exhibits the cyclic voltammetry（CV） curves of all catalysts amid 0 and 1.2 V (vs. RHE) in 0.1 M $HClO_4$ (N_2-saturated). The adsorption and desorption peak of hydrogen can be observed in the region of $0 < E < 0.4$ V, and electrochemical surface area (ECSA) of Pt@Ni ZIF-NC (74 m^2 per g Pt) is almost the same as Pt/C (72 m^2 per g Pt), while that of Pt@ZIF-NC (58 m^2 per g Pt) is lower.

Fig. 4(b) presents the linear sweep voltammetry (LSV) curves of the catalysts. The ORR catalytic performance can be obtained. Their onset potential is in order: Pt@Ni ZIF-NC (1.01 V) > Pt/C (0.94 V) > Pt@ZIF-NC (0.92 V). In terms of half-wave potential ($E_{1/2}$), compared to Pt/C ($E_{1/2}$ = 0.861 V) and Pt@ZIF-NC ($E_{1/2}$ = 0.815 V), there is a significant improvement for Pt@Ni ZIF-NC ($E_{1/2}$ = 0.902 V), which rivals most reported noble metal catalysts (Table S3). The Tafel slope of Pt@Ni ZIF-NC is 69 mV dec^{-1}, lower than that of Pt/C (74 mV dec^{-1}) and Pt@ZIF-NC (98 mV dec^{-1}), suggesting that Pt@Ni ZIF-NC has a faster ORR kinetics (Fig. 4c). To further explore the reaction mechanism of Pt@Ni ZIF-NC, LSV testing under different speeds of 625 rpm to 2500 rpm were performed. As the speed increases, the onset potential remains constant and the current density gradually increases (Fig. S4a). Koutecky-Levich (K-L) diagram of Pt@Ni ZIF-NC shows a very good linear relationship at different potentials (Fig. S4b), indicating the electron transfer number of each oxygen molecule

in the ORR is basically the same. The average electron transfer number of Pt@Ni ZIF-NC is 3.9, demonstrating that its ORR process is highly close to 4 electron transfer. Furthermore, under alkaline conditions (0.1 M KOH), Pt@Ni ZIF-NC also shows higher ORR activity than that of commercial Pt/C and other samples (Fig. S8).

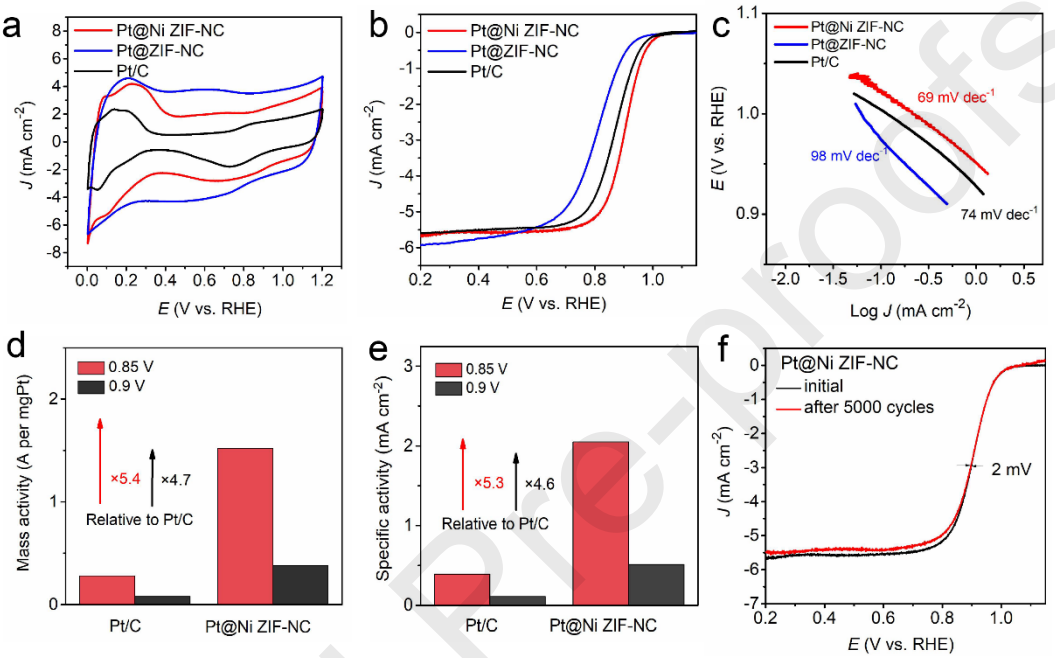

Fig. 4. (a) CV curves recorded in N_2 saturated 0.1 M $HClO_4$ solution. (b) ORR polarization curves and (c) Tafel slopes of Pt@Ni ZIF-NC, Pt@ZIF-NC and Pt/C. (d) Mass activity and (e) specific activity of Pt@Ni ZIF-NC and Pt/C at 0.85 and 0.9 V for ORR. (f) LSV curves of Pt@Ni ZIF-NC before and after 5000 cycles.

In addition, the kinetic current density (J_K) of Pt@Ni ZIF-NC and Pt/C at voltages of 0.9 V and 0.85 V was calculated, the J_K of Pt@Ni ZIF-NC is 6.78 and 27.14 mA cm^{-2}, respectively, greater than that of Pt/C (2.54 and 8.65 mA cm^{-2}). According to J_K, the Pt mass activity of Pt@Ni ZIF-NC was further calculated to be 1.52 A mg^{-1}_{Pt} at 0.85 V (vs. RHE), 5.4 times higher than that of commercial Pt/C catalyst (0.28 A mg^{-1}_{Pt}) (Fig. 4d). When the potential reaches 0.9 V (vs. RHE), its mass activity (0.38

A mg^{-1}_{Pt}) is still 4.7 times than that of Pt/C (0.08 A mg^{-1}_{Pt}). According to Fig. 4(e), the specific activity of Pt@Ni ZIF-NC at 0.85 V (vs. RHE) and 0.9 V are calculated to be 2.1 and 0.51 mA cm^{-2}, which are 5.3 times and 4.6 times higher than that of Pt/C (0.39 mA cm^{-2} at 0.85 V, 0.11 mA cm^{-2} at 0.9 V), respectively.

In addition to excellent activity, the stability test was then measured with accelerating cycling between 0.65 and 1.0 V in O_2 saturated 0.1 M $HClO_4$ solutions. After 5000 cycles, the half-wave potential of Pt@Ni ZIF-NC is only 2 mV less than before (Fig. 4f), whereas it is 23 mV of Pt/C (Fig. S5). After CV accelerated test, compared with the morphology and structure before and after ADT, they are basically stable for Pt@Ni ZIF-NC, and the particle size of Pt NPs keeps almost unchanged (Fig. S6). After 40000 s testing, the normalized current of Pt@Ni ZIF-NC only drops by 9 %, while the current of Pt/C is reduced by 21.6 % after 30000 s (Fig. S7).

3.3. Electrocatalytic performance towards HER

To assess the HER properties, LSV were detected at ambient temperature in 0.5 M H_2SO_4. The Pt loading on the electrode of Pt@Ni ZIF-NC, Pt@ZIF-NC and Pt/C was 1.4, 1.34 and 3.99 μg, respectively. According to iR-compensated LSV curves in Fig. 5(a) (The LSV curves without IR correction are given in Fig. S9), Pt@Ni ZIF-NC shows splendid HER catalytic activity, where the onset potential is only 15 mV. The current density requires merely 29 mV overpotential to achieve 10 mA cm^{-2}, preceding Pt/C (34 mV), Pt@ZIF-NC (34 mV) and the most reported Pt-based catalysts（Fig. 5b, Table S4）. Similarly, the current density barely needs a 37 mV overpotential to reach 50 mA cm^{-2}, while Pt/C and Pt@ZIF-NC require 45 mV and 51

mV overpotentials, respectively. As exhibited in Fig. 5(c), the Tafel slope of Pt@Ni ZIF-NC, Pt@ZIF-NC and Pt/C is 13, 17 and 15 mV dec^{-1}, respectively, demonstrating the rapid HER kinetics of Pt@Ni ZIF-NC. Based on the classical theory, the Tafel mechanism shall be mainly responsible for their HER processes [35,42]. The Nyquist diagram shows that Pt@Ni ZIF-NC has lower charge transfer resistance when compared with Pt@ZIF-NC and Pt/C (Fig. 5d), indicating that the high intrinsic activity of Pt@Ni ZIF-NC. Furthermore, then the mass activity of Pt@Ni ZIF-NC and Pt/C normalized with Pt loading (Fig. 5e) was calculated by LSV curves. As shown in Fig. S10, when the potential is at 20 and 30mV, the mass activity of Pt@Ni ZIF-NC is 0.08 and 0.66 A mg^{-1}_{Pt}, respectively, which is 2 and 6 times as much as that of Pt/C.

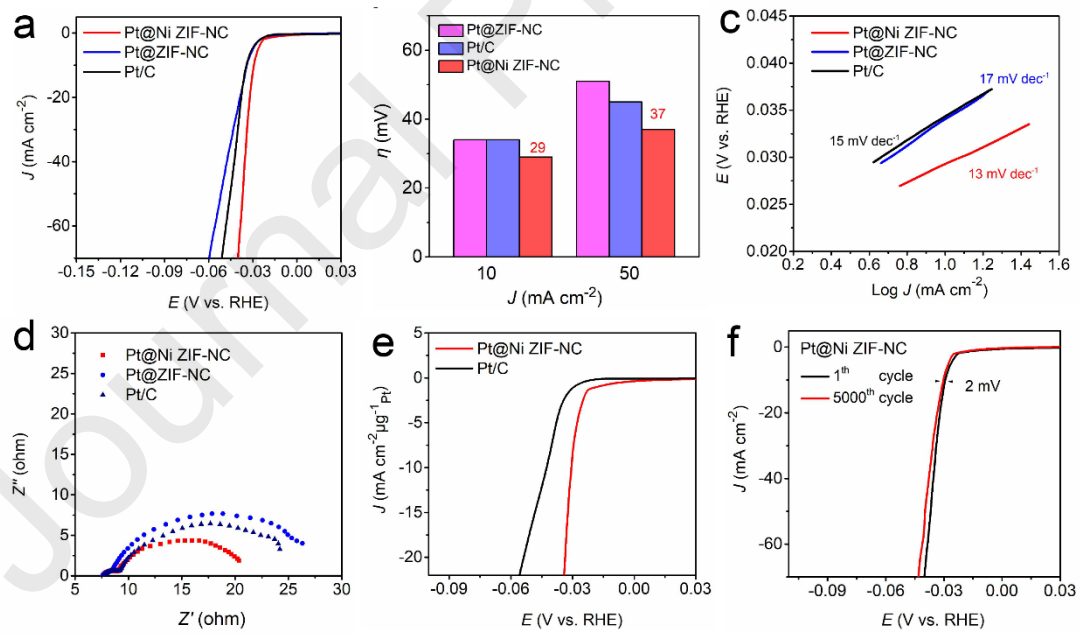

Fig. 5. (a) HER polarization curves of Pt@Ni ZIF-NC, Pt@ZIF-NC and Pt/C in 0.5 M H_2SO_4 electrolyte at a scan rate of 5 mV dec^{-1}. (b) Corresponding overpotentials (j=10/50 mA cm^{-2}). (c) Tafel plots. (d) EIS collected in the frequency range of

0.01–10^5 Hz. (e) LSV curves normalized by loaded Pt on electrodes. (f) LSV curves of Pt@Ni ZIF-NC before and after 5000 CV cycles.

Besides, the stability was further explored. After 5000 cycles, Pt@Ni ZIF-NC is almost overlapped with the original LSV curve (increased by 2 mV) (Fig. 5f), while Pt/C increases by 9 mV after 5000 cycles (Fig. S11). Then, after 50000 s *i–t* test, the normalized current loss of Pt@Ni ZIF-NC is only 6.95%, much smaller than commercial Pt/C (17.82%) after 20000 s (Fig. S12). The above results manifest that Pt@Ni ZIF-NC owns better activity and stability for HER.

3.4. Discussion

For the limit of Ni active sites to Pt NPs, first of all, the structure of the porous carbon matrix provides a suitable place for the dispersion of Ni NPs on it, and finally forms uniformly dispersed Ni sites in the surface of carbon matrix. HRTEM images of Pt@Ni ZIF-NC and Pt@ZIF-NC without Ni species confirm that the Pt NPs in Pt@Ni ZIF-NC have a more uniform and ideal size with a more suitable particle distribution. Compared with Pt@ZIF-NC, the Ni sites of Pt@Ni ZIF-NC do play a role in isolating Pt NPs. Furthermore, the negative shift of Pt 4f peak in Pt@Ni ZIF-NC compared to commercial Pt/C proves the stronger interaction between Ni sites and Pt NPs in Pt@Ni ZIF-NC, which promotes the anchoring of Ni sites onto Pt. Also, the porous carbon can contribute to the confinement of the Pt growth, thus obtaining uniform and ultra-small (2.3 nm) Pt NPs, and thereby increasing the utilization of Pt.

The excellent ORR and HER electrocatalytic activity and stability of Pt@Ni ZIF-NC can be explained as follows: (1) Ultra-small Pt particle size and even

dispersion of Pt NPs are beneficial to enhancing the electrocatalytic performance; (2) Ni ZIF-NC as the support also provides numerous active sites (such as Ni-N_x) for the catalyst, besides, plenty of pyridinic N and graphitic N also has a positive effect on electron transfer and catalytic activity; (3) The synergy between Pt NPs and Ni ZIF-NC in Pt@Ni ZIF-NC further promotes the electrocatalytic performance. Especially for ORR, compared with Pt/C, Pt@ZIF-NC and many other reported Pt-based catalysts, Pt@Ni ZIF-NC has higher half-wave potential, mass activity and stability, which fully demonstrate the synergistic effect.

4. Conclusions

In summary, using the separation effect of Ni sites, the interaction between Ni and Pt and the restriction of Pt NPs in porous carbon matrix, we successfully obtained the well dispersed Pt nanocatalysts with ideal ultra-small particle size. The prepared Pt@Ni ZIF-NC with more active center types and sites, significantly increasing the electrocatalysis efficiency of Pt catalysts. As a result, whether for ORR and HER, it always possesses superior activity and stability than the commercial Pt/C catalyst. In addition, its ORR and HER mass activity beyond Pt/C and most of the literature reports of Pt catalysts. Therefore, our work provides a promising method for designing and constructing highly active and stable next-generation Pt-based catalysts with multiple active centers, which significantly reduces the dosage of Pt. The results show that our Pt@Ni ZIF-NC catalyst has great application prospects in fuel cells and other fields.

Acknowledgments

This work was supported by the National Natural Science Foundation of China (22075223, 51701146), and the State Key Laboratory of Advanced Technology for

Materials Synthesis and Processing (Wuhan University of Technology) (2021-ZD-4).

References

[1] J.R. Kitchin, J.K. Nørskov, M.A. Barteau, J.G. Chen, J. Chem. Phys. 120 (2004) 10240–10246.
[2] D. Zhao, Z. Zhuang, X. Cao, C. Zhang, Q. Peng, C. Chen, Y. Li, Chem. Soc. Rev. 49 (2020) 2215–2264.
[3] E. Luo, Y. Chu, J. Liu, Z. Shi, S. Zhu, L. Gong, J. Ge, C.H. Choi, C. Liu, W. Xing, Energy Environ. Sci. 14 (2021) 2158-2185.
[4] L. Peng, J. Shen, L. Zhang, Y. Wang, R. Xiang, J. Li, L. Li, Z. Wei, J. Mater. Chem. A 5 (2017) 23028–23034.
[5] H. Zhong, Y. Luo, S. He, P. Tang, D. Li, N. Alonso-Vante, Y. Feng, ACS Appl. Mater. Interfaces 9 (2017) 2541–2549.
[6] X. Ao, W. Zhang, B. Zhao, Y. Ding, G. Nam, L. Soule, A. Abdelhafiz, C. Wang, M. Liu, Energy Environ. Sci. 13 (2020) 3032-3040.
[7] D. He, L. Zhang, D. He, G. Zhou, Y. Lin, Z. Deng, X. Hong, Y. Wu, C. Chen, Y. Li, Nat. Commun. 7 (2016) 1–8.
[8] J. Choi, J.H. Jang, C.W. Roh, S. Yang, J. Kim, J. Lim, S.J. Yoo, H. Lee, Appl. Catal. B Environ. 225 (2018) 530–537.
[9] Y. Gu, S. Chen, J. Ren, Y.A. Jia, C. Chen, S. Komarneni, D. Yang, X. Yao, ACS Nano 12 (2018) 245–253.
[10] L. Zhang, K. Doyle-Davis, X. Sun, Energy Environ. Sci. 12 (2019) 492–517.
[11] Z. Song, Y.N. Zhu, H. Liu, M.N. Banis, L. Zhang, J. Li, K. Doyle-Davis, R. Li, T.K. Sham, L. Yang, A. Young, G.A. Botton, L.M. Liu, X. Sun, Small 16 (2020) 1–12. [12] M. Zhao, Z. Chen, Z. Lyu, Z.D. Hood, M. Xie, M. Vara, M. Chi, Y. Xia, J. Am. Chem. Soc. 141 (2019) 7028–7036.
[13] X. Yan, K. Liu, T. Wang, Y. You, J. Liu, P. Wang, X. Pan, G. Wang, J. Luo, J. Zhu, J. Mater. Chem. A 5 (2017) 3336-3345.
[14] X. Yan, K. Liu, T. Wang, Y. You, J. Liu, P. Wang, X. Pan, G. Wang, J. Luo, J. Zhu, J. Mater. Chem. A 5 (2017) 3336–3345.
[15] D. Li, Y. Jia, D. Li, Y. Jia, G. Chang, J. Chen, H. Liu, J. Wang, Y. Hu, Chem 4 (2018) 2345–2356.
[16] Z. Song, M.N. Banis, L. Zhang, B. Wang, L. Yang, D. Banham, Y. Zhao, J. Liang, M. Zheng, R. Li, S. Ye, X. Sun, Nano Energy 53 (2018) 716–725.
[17] S. Liu, H. Bin Yang, S.F. Hung, J. Ding, W. Cai, L. Liu, J. Gao, X. Li, X. Ren, Z. Kuang, Y. Huang, T. Zhang, B. Liu, Angew. Chem. Int. Ed. 59 (2020) 798–803.
[18] X. Huang, L. Cao, Y. Chen, E. Zhu, Z. Lin, M. Li, A. Yan, A. Zettl, Y.M. Wang, X. Duan, T. Mueller, Science 348 (2015) 1230–1234.
[19] H. Jin, H. Zhou, P. Ji, C. Zhang, J. Luo, W. Zeng, C. Hu, D. He, S. Mu, Nano Res. 13 (2020) 818–823.
[20] R. Hao, J.T. Ren, X.W. Lv, W. Li, Y.P. Liu, Z.Y. Yuan, J. Energy Chem. 49 (2020) 14–21.
[21] P.G. Lustemberg, R.M. Palomino, R.A. Gutiérrez, D.C. Grinter, M. Vorokhta, Z.

Liu, P.J. Ramírez, V. Matolín, M.V. Ganduglia-Pirovano, S.D. Senanayake, J.A. Rodriguez, J. Am. Chem. Soc. 140 (2018) 7681–7687.

[22] M. Liu, X. Yin, X. Guo, L. Hu, H. Yuan, G. Wang, F. Wang, L. Chen, L. Zhang, F. Yu, Nano Mater. Sci. 1 (2019) 131–136.
[23] P. Ji, H. Jin, H. Xia, X. Luo, J. Zhu, Z. Pu, S. Mu, ACS Appl. Mater. Interfaces 12 (2020) 727–733.
[24] D. Chen, J. Zhu, X. Mu, R. Cheng, W. Li, S. Liu, Z. Pu, C. Lin, S. Mu, Appl. Catal. B Environ. 268 (2020) 118729.
[25] B. Wang, C. Tang, H.F. Wang, X. Chen, R. Cao, Q. Zhang, J. Energy Chem. 38 (2019) 8–14.
[26] L. Zhang, Y. Zheng, J. Wang, Y. Geng, B. Zhang, J. He, J. Xue, T. Frauenheim, M. Li, Small 17 (2021) 1–11.
[27] C. Hu, H. Jin, B. Liu, L. Liang, Z. Wang, D. Chen, D. He, S. Mu, Nano Energy 82 (2021) 105714.
[28] M. Liu, L. Wang, K. Zhao, S. Shi, Q. Shao, L. Zhang, X. Sun, Y. Zhao, J. Zhang, Energy Environ. Sci. 12 (2019) 2890–2923.
[29] F. Kong, Z. Ren, M. Norouzi Banis, L. Du, X. Zhou, G. Chen, L. Zhang, J. Li, S. Wang, M. Li, K. Doyle-Davis, Y. Ma, R. Li, A. Young, L. Yang, M. Markiewicz, Y. Tong, G. Yin, C. Du, J. Luo, X. Sun, ACS Catal. 10 (2020) 4205-4214.
[30] X.F. Lu, B.Y. Xia, S.Q. Zang, X.W. Lou, Angew. Chem. Int. Ed. 59 (2020) 4634–4650.
[31] Z. Pu, Q. Liu, A.M. Asiri, X. Sun, ACS Appl. Mater. Interfaces 6 (2014) 21874–21879.
[32] P. Liu, D. Gao, W. Xiao, L. Ma, K. Sun, P. Xi, D. Xue, J. Wang, Adv. Funct. Mater. 28 (2018) 1706928.
[33] X. Wang, A. Vasileff, Y. Jiao, Y. Zheng, S.Z. Qiao, Adv. Mater. 31 (2019) 1–8.
[34] P. Wang, K. Jiang, G. Wang, J. Yao, X. Huang, Angew. Chem. Int. Ed. 55 (2016) 12859–12863.
[35] C. Zhang, P. Wang, W. Li, Z. Zhang, J. Zhu, Z. Pu, Y. Zhao, S. Mu, J. Mater. Chem. A. 8 (2020) 19348–19356.
[36] S. Yuan, Z. Pu, H. Zhou, J. Yu, I.S. Amiinu, J. Zhu, Q. Liang, J. Yang, D. He, Z. Hu, G. Van Tendeloo, S. Mu, Nano Energy 59 (2019) 472-480.
[37] J. Zhang, Y. Yuan, L. Gao, G. Zeng, M. Li, H. Huang, Adv. Mater. 2006494 (2021) 1–23.
[38] T.H. Vuong, N. Rockstroh, U. Bentrup, J. Rabeah, J. Knossalla, S. Peitz, R. Franke, A. Brückner, ACS Catal. 11 (2021) 3541–3552.
[39] X. Liu, L. Zheng, C. Han, H. Zong, G. Yang, S. Lin, A. Kumar, A.R. Jadhav, N.Q. Tran, Y. Hwang, J. Lee, S. Vasimalla, Z. Chen, S.G. Kim, H. Lee, Adv. Funct. Mater. 2100547 (2021) 1–9.
[40] S. Wei, A. Li, J.C. Liu, Z. Li, W. Chen, Y. Gong, Q. Zhang, W.C. Cheong, Y. Wang, L. Zheng, H. Xiao, C. Chen, D. Wang, Q. Peng, L. Gu, X. Han, J. Li, Y. Li, Nat. Nanotech. 13 (2018) 856–861.
[41] H. Li, Y. Wen, M. Jiang, Y. Yao, H. Zhou, Z. Huang, J. Li, S. Jiao, Y. Kuang, S.

Luo, Adv. Funct. Mater. 2011289 (2021) 1–13.
[42] C. Zhang, X. Liang, R. Xu, C. Dai, B. Wu, G. Yu, B. Chen, X. Wang, N. Liu, Adv. Funct. Mater. 2008298 (2021) 1–11.

Graphical abstract

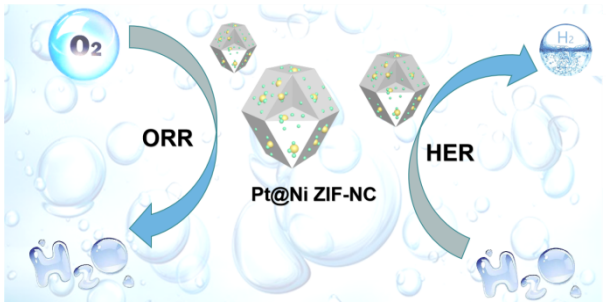

Using Ni sites in Ni ZIF-NC to isolate Pt, the obtained Pt@Ni ZIF-NC catalyst, with ultrasmall, uniform and highly dispersed Pt nanoparticles, presents highly efficient and stable dual-functional catalysis toward oxygen reduction and hydrogen evolution reactions.

- The Ni site can isolate Pt nanoparticles and own strong interaction with Pt in Pt@Ni ZIF-NC catalysts.
- There is a synergistic effect between Ni sites and Pt nanoparticles.
- Pt@Ni ZIF-NC, with uniform and highly dispersed Pt nanoparticles, exhibits greatly enhanced ORR performance in acidic media.
- High HER performance is also obtained for Pt@Ni ZIF-NC in acidic media.
- It provides a promising method for designing highly active, stable ultrasmall and ultralow Pt-loaded catalysts.